

## Synthesis and Characterisation of Carbon Aerogel Derived from Carboxymethyl Cellulose as Hydrogen Storage Material

Ahmad Solehin Ab Sabar,<sup>1</sup> Syaza Azhari,<sup>1\*</sup> Nur Atiqah Nasir<sup>1</sup> and Muhammad Zamir Othman<sup>2,3</sup>

<sup>1</sup>Faculty of Science and Technology, Universiti Sains Islam Malaysia, Bandar Baru Nilai, 71800 Nilai, Negeri Sembilan, Malaysia

<sup>2</sup>Infinite Opportunities Sdn. Bhd., 11, Lorong Astana 1A/KU2, Bandar Bukit Raja, 41050 Klang, Selangor, Malaysia

<sup>3</sup>Sugarbomb Worldwide Sdn. Bhd., 9, Lorong Astana 1A/KU2, Bandar Bukit Raja, 41050 Klang, Selangor, Malaysia

\*Corresponding author: syaza@usim.edu.my

Published online: 25 August 2023

To cite this article: Ahmad Solehin, A. S. et al. (2023). Synthesis and characterisation of carbon aerogel derived from carboxymethyl cellulose as hydrogen storage material. *J. Phys. Sci.*, 34(2), 13–27. <https://doi.org/10.21315/jps2023.34.2.2>

To link to this article: <https://doi.org/10.21315/jps2023.34.2.2>

**ABSTRACT:** *A direct, simple and low-cost approach to synthesising carbon aerogel-magnesium (CA-Mg) composites has been demonstrated in this research. It is conducted by carbonising sodium carboxymethyl cellulose (CMC) aerogels via a sol-gel and freeze-drying process. Mg is used as an enhancer for CA in the preparation step and as a selective candidate for the hydrogen storage device. Note that the structure and morphology of CA-Mg composites are characterised using field emission scanning electron microscopy (FESEM), fourier transforms infrared spectroscopy (FTIR) and X-ray diffraction (XRD) techniques. The ability of CA-Mg composites to act as a hydrogen storage device is analysed by utilising Brunauer-Emmett-Teller (BET) and temperature-programmed desorption analysis. The CA-Mg composites comprise porous structures with a high specific surface area of 101.4407 m<sup>2</sup>/g, and 0.002 mol of Mg<sup>2+</sup> is the optimum concentration for synthesising CA-Mg composites. As a potential candidate for a hydrogen storage device, the CA-Mg composites show an initial dehydrogenation temperature of 377.22°C, where they desorbed the maximum amount of hydrogen gas. This study emphasises the potential for using CA as a hydrogen storage device, which fulfils the seventh goal of the Sustainable Development Goals (SDGs), affordable and clean energy, as well as Department of Energy (DOE)'s goal of using carbon-based materials.*

**Keywords:** carbon aerogel, carboxymethyl cellulose, carbonisation, hydrogen storage

## 1. INTRODUCTION

Nowadays, when it comes to energy demand, many efforts have been made to ensure the continuity of the energy supply. This is due to the high dependence on depleting fossil fuel sources, global economic expansion and climate change.<sup>1</sup> Many researchers have devised different ideas for converting energy storage from renewable sources. Note that these ideas focus on making devices that use less energy and are environmentally friendly. One of the best alternatives is hydrogen energy obtained from water, which can be discovered almost everywhere. Hence, it is the best solution for energy challenges where it can be produced continuously. The most promising characteristics of hydrogen energy are that it is non-toxic and environmentally safe. Unfortunately, the first challenge is to store hydrogen gases in designated materials.<sup>2</sup> Various methods have been developed to store hydrogen, especially via sorbents such as carbon-based materials. For example, carbon aerogel (CA) is a carbon-based material with promising characteristics as hydrogen storage due to its high specific area and porous structure.<sup>2,3</sup> These characteristics have made CA a potential candidate for hydrogen storage applications. Other than that, CA can be synthesised from sodium carboxymethyl cellulose (CMC) through several processes, such as gelation, freeze-drying and carbonisation. These processes are simple and can be considered green techniques. Conventionally, CA comprises the carbonisation of organic aerogels such as phenol/formaldehyde aerogels and cresol/formaldehyde aerogels. However, the disadvantages of using these methods are that they are expensive, utilise toxic carbon sources and involve complicated synthesis processes, making them less suitable for mass production and commercialisation due to safety concerns.<sup>1,4-6</sup>

Various research has recently been performed utilising cellulose sources due to their renewability and biocompatibility. Researchers choose cellulose as their research subject because it is plentiful, making it renewable, sustainable and environmentally friendly. Moreover, CMC can be applied in preparing CA as a starting precursor, which must undergo several processes, starting with gelation, solvent exchange, freeze drying and finally, pyrolysis. All steps involved are simple and can be deemed to be green techniques.<sup>2,7</sup> CMC is a non-toxic, biocompatible and water-soluble cellulose derived from carboxymethylation of the hydroxyl group in cellulose molecules. Due to the carboxyl groups' presence, CMC can be cross-linked with metal ions to enhance its properties.<sup>1,4,5</sup> Attributable to the promising potential of CA in energy storage applications, substantial work involving the fabrication of CA cross-linked with metal ions has been conducted. For example, the derivation of CA/nickel(II) oxide (NiO) composites and the preparation of sodium polyacrylate functionalised carbon nanotube aerogels.<sup>1,8</sup>

Carbon-based materials are the most suitable for gas storage due to their very small pores, high porosity and attractive force between carbon atoms and gas molecules.<sup>2</sup> The features of CA, such as its high porosity, make it ideal for hydrogen energy storage. Apart from that, an adsorption process is involved in storing hydrogen via the physical bonding of van der Waals forces between materials with a high surface area and molecular hydrogen.<sup>9,10</sup> Different adsorbents can store hydrogens, such as carbon-based materials, zeolites and metal-organic frameworks (MOFs). Nevertheless, most of them have low densities and require additives for heat conductivity optimisation due to the limitation on the density levels of hydrogen to be stored, which needs to be greater than 40 kg/m<sup>3</sup>–50 kg/m<sup>3</sup>. Note that it is not easy to achieve by employing available adsorbents.<sup>5,11–13</sup> Previous research presents that the standard set by the Department of Energy (DOE), where the storage must be at least 6 wt% for application in the transportation industry, could not be achieved. The current research on carbon-based materials indicates a 5.5 wt% hydrogen uptake at room temperature, considered the best to meet DOE's standard.<sup>14</sup> Hence, research on carbon-based materials needs to be explored and varied to achieve DOE's standard by synthesising CA-Mg composites via direct pyrolysis of CMC aerogels. CMC aerogels are prepared beforehand through the sol-gel process and freeze-drying by adding magnesium dichloride (MgCl<sub>2</sub>) as a cross-linking agent. Consequently, the synthesised CA-Mg composites have a high surface area and a porous structure, which can be suggested as a potential solution for hydrogen storage devices.<sup>15–17</sup>

## 2. EXPERIMENTAL

### 2.1 Materials

Sodium CMC (NaCMC) was bought from Chemiz (Selangor, Malaysia). Meanwhile, Magnesium (II) chloride (MgCl<sub>2</sub>.6H<sub>2</sub>O), sodium hydroxide (NaOH), D-(+)-gluconic acid-lactone (GDL) and glycerol (C<sub>3</sub>H<sub>8</sub>O<sub>3</sub>) were bought from Sigma-Aldrich (Selangor, Malaysia).

### 2.2 Synthesis of CA from CMC

Firstly, 4% of CMC aerogels were prepared by weighing commercial grade NaCMC, D-(+)-GDL and glycerol in a ratio of 8:4:1 and dissolving them in 200 ml of deionised water. For 30 min, the blend was stirred under magnetic stirring at room temperature until a transparent solution was attained. Besides, MgCl<sub>2</sub> solutions with various concentrations (0.002 mol, 0.004 mol, 0.006 mol, 0.008 mol and 0.01 mol) were prepared in 5.5 ml of distilled water and 0.5 ml of a 0.01 M

NaOH solution. Correspondingly, each concentration was mixed with the NaOH solution and stirred until a homogenous solution was obtained. Subsequently, the  $\text{MgCl}_2$  solutions were blended with the obtained CMC solution and stirred for 5 min to ensure homogeneity. The mixed gel solutions were poured into a cylindrical polystyrene tubule and left at room temperature for 3 days to encourage the gelation and cross-linking reactions. Lastly, the gels underwent freeze-drying at  $-50^\circ\text{C}$  for 60 h to obtain the CMC aerogels. The CMC aerogels were then turned into CA by carbonising them in a tube furnace at  $800^\circ\text{C}$  for 2 h at a heating rate of  $5^\circ\text{C}/\text{min}$  under a nitrogen ( $\text{N}_2$ ) atmosphere.

### 2.3 Characterisation of CA

The morphology of CA surfaces was examined using FESEM (JSM IT 800 SHL, Japan) with different concentrations of metal ion solutions. The changes in structure were compared between samples doped with metal ions and those without metal ions. Consequently, the samples were sputter-coated beforehand with a thin layer of gold before observation bombarded with 1 KeV of electrons. The electrons emitted from the samples with the energy of 1 KeV were defined as secondary electrons and used for sample investigation.<sup>18</sup> The FTIR (Thermo Scientific Nicolet iS50R, United States) was utilised to detect the presence of a functional group. The changes in the samples were observed to determine the completion of carbonisation, where most of the molecular bonds were destroyed during carbonisation. Note that the FTIR spectra were recorded from 8 scans at a resolution of  $4\text{ cm}^{-1}$  between  $4,000\text{ cm}^{-1}$ – $400\text{ cm}^{-1}$ . The spectra were observed, and peak formation was labelled accordingly. The crystal structure of the samples was characterised using (XRD [Rigaku MiniFlex 600, Japan]). The XRD patterns of the samples were examined at a  $2\theta$  range of  $2^\circ$  to  $90^\circ$  to determine the presence of any metal oxide formed during carbonisation.<sup>19</sup>

### 2.4 The Ability of CA as a Hydrogen Storage

The ability of the samples to act as hydrogen storage was analysed using Brunauer-Emmett-Teller (BET) (Micromeritics 3Flex, United States) and Temperature Programmed Desorption (TPD) (Micromeritics 3Flex, United States) analysis. From the BET analysis, the samples' specific surface area and pore size were determined, and the samples that met the desired criteria were chosen. This analysis was executed by the nitrogen adsorption/desorption method using the surface area analyser. Correspondingly, the samples were dried sufficiently during the degassing technique to avoid negative interference between the sample and  $\text{N}_2$  gas. For porosity measurement,  $\text{N}_2$  gas was employed as a physisorption gas. The samples were backfilled with helium (He) and allowed

to cool to room temperature.<sup>20</sup> All data were analysed using 3Flex version 5.02 software. Consequently, a temperature range of TPD-Hydrogen analysis was used to investigate the desorption behaviour of hydrogen storage materials.<sup>21,22</sup> Thermo scientific analysed different concentrations of the prepared samples based on the desorption behaviour of hydrogen towards the samples using TPD/R/O 1100. All the information regarding the samples was collected from the software.

### 3. RESULTS AND DISCUSSION

#### 3.1 Synthesis of CA from CMC

CA was derived from commercial-grade CMC by preparing a CMC solution and mixed with  $\text{MgCl}_2$  to form hydrogels. The hydrogels with different concentrations (0.002 mol, 0.004 mol, 0.006 mol, 0.008 mol and 0.01 mol) of  $\text{MgCl}_2$  were freeze-dried and CMC- $\text{MgCl}_2$  aerogels were formed in the form of a white spongy structure. Other than that, the structure became spongier as the concentration increased. These aerogels with different concentrations were carbonised in a tube furnace for 2 h at  $800^\circ\text{C}$  to prepare CA. Table 1 indicates the weight differences between the aerogel samples. Each sample was repeated several times with a consistent weight loss percentage. Note that the percentage weight loss of the samples increased when the concentration of  $\text{MgCl}_2$  increased. This happened due to the decomposition of the anion that acted as an oxidising agent for the CA.<sup>1,23</sup> In this research, CA-Mg oxidised  $\text{MgCl}_2$  into  $\text{MgO}$  during carbonisation. This explained why the percentage weight loss was the lowest at 0.002 mol because  $\text{MgO}$  was less generated at that concentration.

Table 1: Percentage of weight loss of CA-Mg samples.

Samples	Concentration (mol)	Average percentage weight loss (%)	Relative standard deviation (%)
CA	–	64.54	7.82
CA-Mg	0.002	53.55	4.80
	0.004	56.27	4.40
	0.006	58.56	4.11
	0.008	58.60	1.97
	0.010	64.07	4.53

### 3.2 FTIR Analysis

Figure 1(a) illustrates the FTIR spectra of CMC-MgCl<sub>2</sub> before carbonisation and pure MgCl<sub>2</sub>. The presence of -OH stretch was exhibited at 3,356 cm<sup>-1</sup> and 3,371 cm<sup>-1</sup> for MgCl<sub>2</sub> and CMC-MgCl<sub>2</sub>, respectively. On the other hand, Figure 1(b) demonstrates the FTIR spectra of pure CA and CA-Mg with different concentrations of MgCl<sub>2</sub>. The IR spectrum of pure CA (Figure 1[a]) portrays the presence of the -OH stretches at 3,332 cm<sup>-1</sup>. Meanwhile, no peak was shown at the same wavenumber for CA-Mg (Figure 1[b]), indicating that either the MgCl<sub>2</sub> became anhydrous or decomposed into another compound. Here, the CA-Mg spectra did not indicate any significant peaks since most of the functional groups in CMC have been decomposed during the carbonisation process. The FTIR spectra comparisons in Figure 1(a) and Figure 1(b) prove the completeness of carbonisation for CMC aerogel. With the addition of MgCl<sub>2</sub> as a Mg precursor, the carbonisation became complete as fewer peaks were observed compared to pure CA (Figure 1[b]).

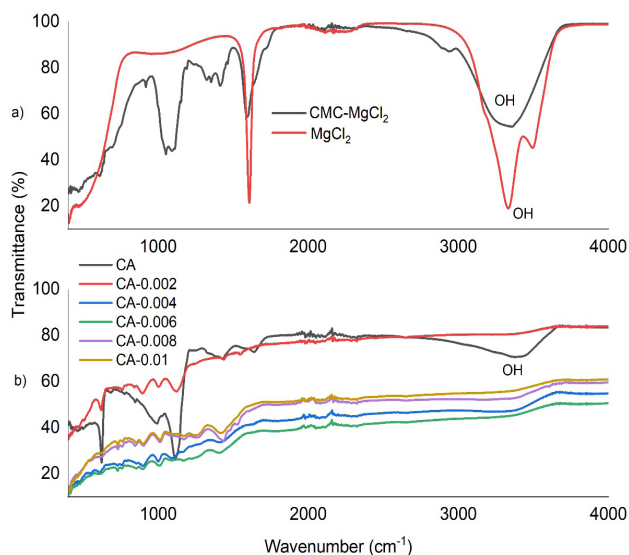
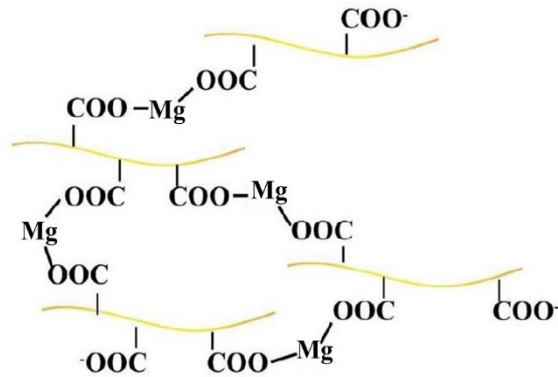


Figure 1: FTIR Spectra of (a) CMC-MgCl<sub>2</sub> aerogel and MgCl<sub>2</sub> (b) CA and CA-Mg.

Furthermore, Figure 1(a) depicts the FTIR spectra of CMC-MgCl<sub>2</sub> and pure MgCl<sub>2</sub>. These spectra indicated the presence of the carboxylate group (CO) at 1,051 cm<sup>-1</sup>, the main factor for the cross-linking reaction. The large number of CO on CMC molecular chains caused Mg<sup>2+</sup> to react with the CO during the sol-gel process, resulting in a cross-linked network structure.<sup>9</sup> This can be explained from Scheme 1.



Scheme 1: Mechanism of cross-linking reaction for the CMC-MgCl<sub>2</sub> aerogels.

### 3.3 XRD Analysis

Figure 2 represents the XRD patterns of CA-Mg samples in the  $2\theta$  range of  $20^\circ$ – $90^\circ$ . The samples were tested with five different concentrations of MgCl<sub>2</sub> (0.002 mol, 0.004 mol, 0.006 mol, 0.008 mol and 0.01 mol), and similar patterns were observed. Based on the pattern, the diffraction peaks of MgO (periclase) emerged at  $2\theta$  of  $39^\circ$ ,  $45.5^\circ$ ,  $66.2^\circ$ ,  $79.7^\circ$  and  $84^\circ$  presenting the crystalline phase of MgO, indexed as the (111), (200), (220), (311) and (222) lattice planes. Subsequently, the diffractogram peak was determined based on the XRD profile pattern of periclase. Periclase (MgO) was the only existing crystalline form of MgO.<sup>24</sup> MgO was generated during the carbonisation process of CA-Mg samples. Hence, this is why the disappearance of the OH peak in the FTIR spectra is depicted in Figure 1(b). The MgCl<sub>2</sub> had been decomposed into MgO.<sup>1</sup> Thus, the sample was proven to have CA and MgO characteristic features. The concentration of Mg<sup>2+</sup> influenced the formation of periclase and led to a slight increase in peak intensity. Besides, the peak intensity may not be visible in the XRD pattern at low concentrations (111) and (311).

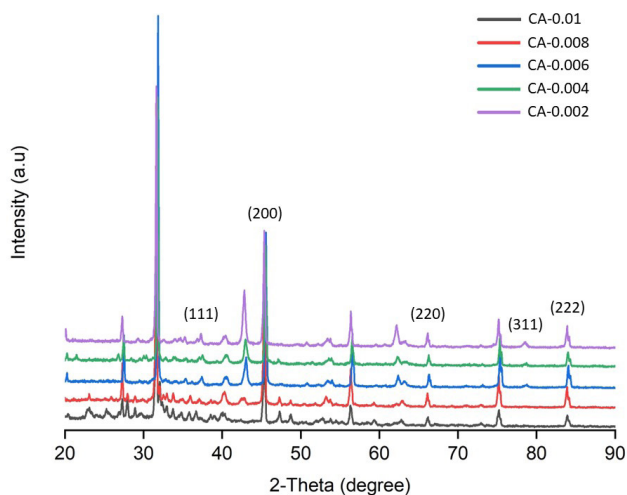


Figure 2: XRD patterns of CA-Mg samples.

### 3.4 FESEM Analysis

The morphology of CA-Mg samples was observed utilising FESEM micrographs (Figure 3). Each sample with a different concentration displayed different morphology in terms of porosity. Nevertheless, the structure was poorly developed for the pure CA sample (untreated  $\text{MgCl}_2$ ), and fewer pores were observed (Figure 3[a]). At 0.002 mol, the porosity increased and was well-structured, while at 0.004 mol and 0.006 mol, denser pores were observed. The structure drastically collapsed, and the porosity became denser as the concentration increased to 0.008 mol and 0.01 mol (Figure 3[d], Figure 3[e] and Figure 3[f]). This is the major effect of the cross-linking reaction between  $\text{Mg}^{2+}$  and CMC molecules during aerogel synthesis. Correspondingly, this reaction led to the formation of a cross-linked network structure.<sup>1,25</sup> During freeze-drying, it may affect the structure of the ice formed, the water vapour during primary drying, and the quality of the final dried product.<sup>26</sup> In Figure 3(a), Figure 3(b) and Figure 3(c), the samples might experience this effect, causing a network structure with large pores. It was recommended to work with high freezing rates to avoid internal water vapour diffusion and form a more homogenous pore size distribution.<sup>26</sup> Further analysis of the porosity is conducted using BET analysis.

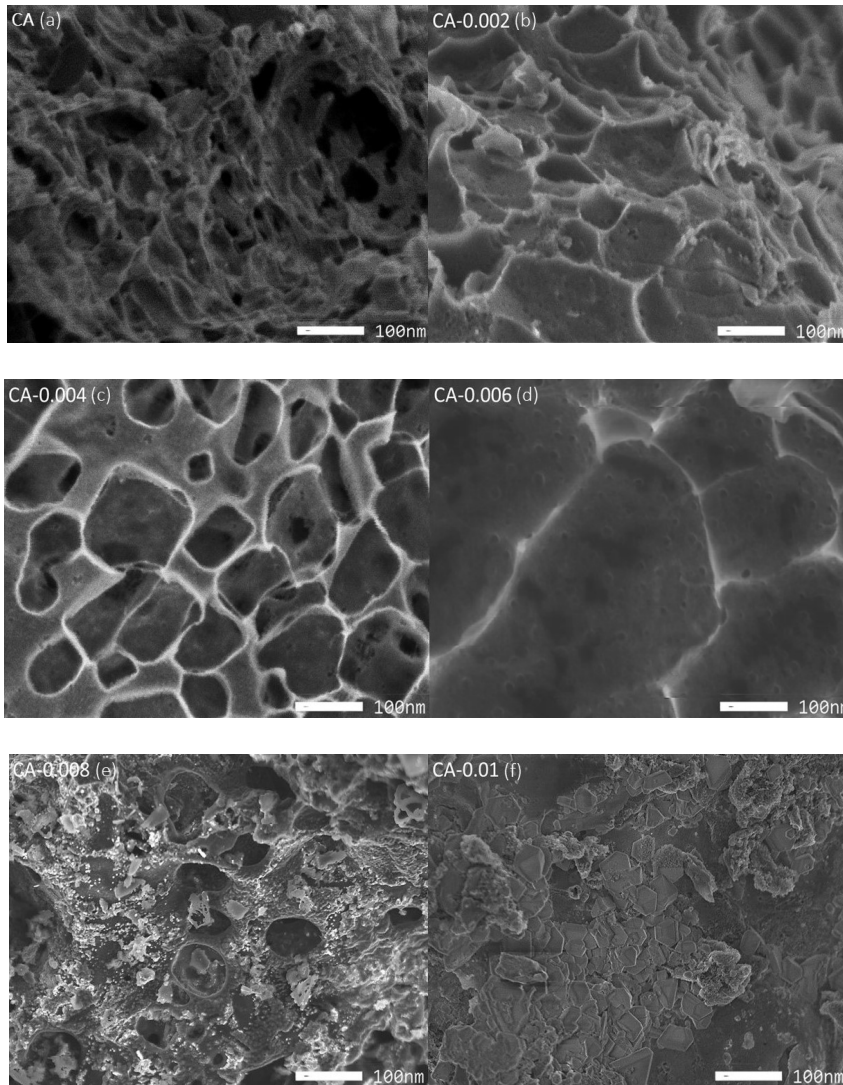


Figure 3: FESEM images of (a) CA, (b) CA-0.002, (c) CA-0.004, (d) CA-0.006, (e) CA-0.008 and (f) CA-0.01.

### 3.5 BET Analysis

The  $N_2$  adsorption/desorption experiments were determined using BET methods to investigate the CA and CA-Mg samples' specific surface area and pore size distribution (Figure 4). According to the International Union of Pure and Applied Chemistry (IUPAC) classification, each sample exhibited typical IV adsorption/

desorption isotherms. This analysis was indicated in the relative pressure region of  $0.4 < P/P_0 > 1.0$ , where each sample displayed a clear hysteresis loop in the region and indicated the existence of mesopores (pore size 2 nm to 50 nm).<sup>1</sup> Other than that, the pore structural parameters and specific capacities of the CA and CA-Mg samples, where the contribution of micropores (pore sizes up to 2 nm) can be calculated (Table 2). The CA-0.002 sample presented a maximum specific surface area of  $101.4407 \text{ m}^2/\text{g}$ , which will probably become a factor in the increased occurrence of the cross-linking reaction, leading to the formation of many pores during the pyrolysis process.<sup>1</sup> The CA sample indicated the lowest pore volume of  $0.0275 \text{ cm}^3/\text{g}$ , while the CA-Mg samples had larger pore volumes of  $0.0893 \text{ cm}^3/\text{g}$ ,  $0.0965 \text{ cm}^3/\text{g}$ ,  $0.1186 \text{ cm}^3/\text{g}$ ,  $0.1216 \text{ cm}^3/\text{g}$  and  $0.1327 \text{ cm}^3/\text{g}$ , respectively. From Table 2, the micropore volume of CA contributed 29.9% of the pore volume, while for CA-0.01, the contribution of micropores was 7.5% of the pore volume. Therefore, the CA-0.01 sample possessed the highest value of pore volume, which is  $0.1327 \text{ cm}^3/\text{g}$ , and the most probable pore size of 11.6339 nm. These features of CA-0.01 could offer a good adsorption site for hydrogen gas and could act as a potential candidate for a hydrogen storage device.<sup>27</sup> On the other hand, FESEM images (Figure 3) of the CA samples portray the differences in morphology of each sample in terms of porosity, where the density of porosity kept increasing as the concentration of  $\text{Mg}^{2+}$  increased. The differences can be observed from BET analysis. Note that the contribution of micropores was lessened as the concentration of  $\text{Mg}^{2+}$  increased. The increased contribution of mesopores helped offer a good adsorption site for hydrogen gas.

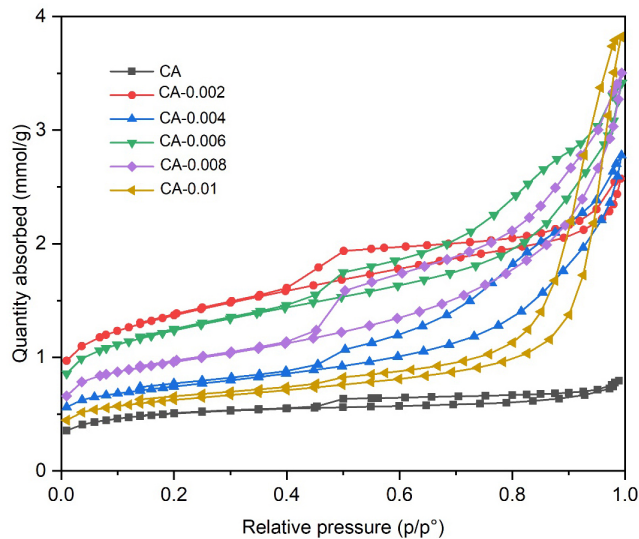


Figure 4: Nitrogen adsorption/desorption isotherms of CA and CA-Mg samples.

Table 2: The pore structural parameters and specific capacity of the CA and CA-Mg samples.

Samples	$S_{\text{BET}}$ ( $\text{m}^2/\text{g}$ )	$S_{\text{mic}}$ ( $\text{m}^2/\text{g}$ )	$V_{\text{total}}$ ( $\text{cm}^3/\text{g}$ )	$V_{\text{mic}}$ ( $\text{cm}^3/\text{g}$ )	Contribution of Mic (%)	D (nm)
CA	36.3241	15.1654	0.0275	0.0082	29.9	3.0379
CA-0.002	101.4407	33.6572	0.0893	0.0179	20.1	3.5240
CA-0.004	54.3267	23.6874	0.0965	0.0124	12.9	7.1064
CA-0.006	91.8824	29.9439	0.1186	0.0158	13.4	5.1644
CA-0.008	70.6374	27.7358	0.1216	0.0145	11.9	6.8913
CA-0.010	45.6454	18.6878	0.1327	0.0098	7.5	11.6339

### 3.6 TPD Analysis

The desorption behaviours of CA and CA-Mg samples as hydrogen storage materials were observed over a wide temperature range using TPD analysis. Figure 5 presents the TPD curves of CA and CA-Mg samples from room temperature to 500°C. It can be observed that hydrogen desorption occurred on CA and CA-Mg samples. Here, the TPD curve profiles for each sample suggested the different initial dehydrogenation temperatures where the presence of  $\text{Mg}^{2+}$  became the main factor. The pure CA began to release hydrogen at 367.81°C, whereas the initial dehydrogenation temperature of CA-Mg increased first at 377.22°C (0.002 mol) and 377.33°C (0.004 mol). Subsequently, it decreased to 372.69°C (0.006 mol) and finally to 346.76°C (0.008 mol). However, the dehydrogenation temperature increased back to 411.15°C at 0.01 mol.

Regarding the percentage of hydrogen released, CA and CA-0.002 indicated a significant TPD curve consisting of two desorption peaks. The first desorption of CA occurred after 44 min at 0.163%, and the second desorption occurred after 7 min at 0.158%. For CA-0.002, the first desorption took 47 min at 0.168%, and the second took 4 min at 0.167%. Even after the second desorption, CA-0.002 released the most hydrogen compared to CA. Compared to CA, CA-0.002 has the most efficient method of releasing hydrogen, with the second desorption taking only 4 min. This happened due to the different contributions of micropore volume decreasing in each sample, as presented in Table 2. Note that the contribution of micropore volume becomes lower as the concentration of Mg increases. The increase in the concentration of  $\text{Mg}^{2+}$  has led to the formation of mesopore in CA-Mg samples, which is the main feature of hydrogen storage materials. This has been indicated by BET analysis that adding  $\text{Mg}^{2+}$  can enhance the hydrogen desorption behaviour of CA, depending on the concentration of  $\text{Mg}^{2+}$ .

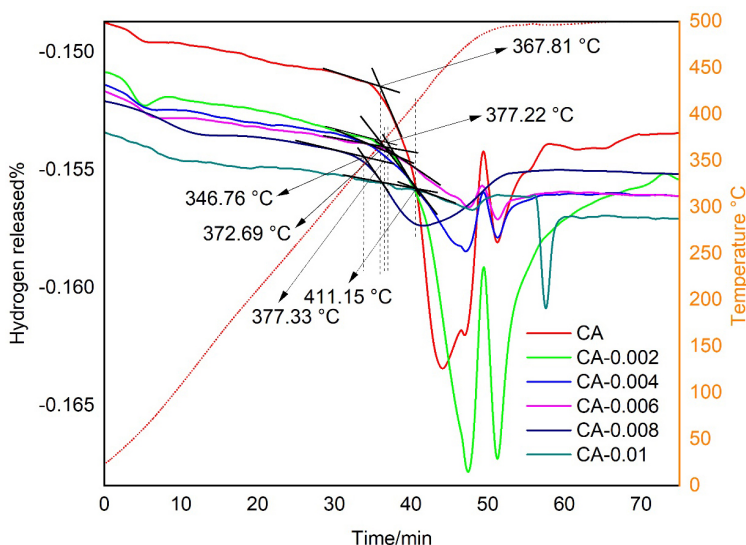


Figure 5: TPD curves of CA and CA-Mg samples from room temperature to 500°C with the ramp rate of 10°C min<sup>-1</sup>.

#### 4. CONCLUSION

In the current research, a simple method has been successfully applied to synthesising CA-Mg composites using NaCMC as a carbon precursor and Mg chloride as a Mg source for the metal ion cross-linking process. The synthesis involved a few simple steps, starting with the sol-gel process, freeze-drying and completion with the carbonisation process. Note that the main product is CA, enhanced with MgO, and contributes to forming a porous structure and a high specific surface area (101.4407 m<sup>2</sup>/g). These features could offer CA an excellent adsorption site for hydrogen gas and could act as a potential candidate for a hydrogen storage device. Moreover, the CA samples released the most hydrogen gas at 0.002 mol compared to the other concentration, where the initial dehydrogenation temperature was 377.22°C. It took 47 min to release hydrogen at 0.168% and another 4 min at 0.167%. Hence, CA-0.002 has the most efficient way of desorbing hydrogen, and 0.002 mol can be considered the optimum condition for synthesising CA as a hydrogen storage material since it can desorb the maximum amount of hydrogen gas. The existence of micropores was crucial, as CA-0.002 desorbed hydrogen the most, even though it had a higher micropore volume and surface area than the other samples. Therefore, a direct, simple and

low-cost step in synthesising CA-Mg composites has been anticipated to be a promising candidate for enhancement and future needs of hydrogen storage devices.

## 5. ACKNOWLEDGEMENTS

This work was supported by the Ministry of Higher Education Malaysia for financial support through the Fundamental Research Grant Scheme (Grant Code: USIM/FRGS/FST/055002/51519). We also thank the Faculty of Science and Technology, Department of Chemistry, Universiti Sains Islam Malaysia, for providing research facilities.

## 6. REFERENCES

1. Yu, M. et al. (2017). One-step synthesis of sodium carboxymethyl cellulose-derived carbon aerogel/nickel oxide composites for energy storage. *Chem. Eng. J.*, 324, 287–295. <https://doi.org/10.1016/j.cej.2017.05.048>
2. Kayfeci, M. & Keçebaş, A. (2019). Hydrogen storage. *Solar Hydro. Produc. Proc., Sys. Technol.*, 85–110. <https://doi.org/10.1016/B978-0-12-814853-2.00004-7>
3. Clark, W. R. et al. (2019). Sorbents. In Ronco, C. et al. (3rd Eds.). *Critical Care Nephrology*. Elsevier, 1137–1154.e2. <https://doi.org/10.1016/B978-0-323-44942-7.00189-8>
4. Ergun, R. et al. (2015). Cellulose. *Encyclo. Food Health*, 694–702. <https://doi.org/10.1016/B978-0-12-384947-2.00127-6>
5. Alizadeh Asl, S. et al. (2017). Synthesis and characterisation of carboxymethyl cellulose from sugarcane bagasse. *J. Food Process. Technol.*, 8(8). <https://doi.org/10.4172/2157-7110.1000687>
6. Aravamudhan, A. et al. (2014). Natural polymers. In Sangamesh, G. K. Laurencin, C. T. Deng, M. (Eds.). *Natural and Synthetic Biomedical Polymers*. Elsevier, 67–89. <https://doi.org/10.1016/B978-0-12-396983-5.00004-1>
7. Li, X. et al. (2020). Preparation of hydrogen storage carbon materials using bio-oil heavy components as carbon-containing precursor. *Fuel Process. Technol.*, 203, 106386. <https://doi.org/10.1016/j.fuproc.2020.106386>
8. Fest, A. et al. (2023). Metal decorated carbon nanotube aerogels from sodium polyacrylate crosslinking by divalent ions. *Carbon Trends*, 10, 100235. <https://doi.org/10.1016/j.cartre.2022.100235>
9. Pandey, A. P. et al. (2020). Hydrogen storage properties of carbon aerogel synthesised by ambient pressure drying using new catalyst triethylamine. *Int. J. Hydrogen Energy*, 45(55), 30818–30827. <https://doi.org/10.1016/j.ijhydene.2020.08.145>

10. Liu, Y. et al. (2013). Study on hydrogen storage properties of Mg nanoparticles confined in carbon aerogels. *Int. J. Hydrogen Energy*, 38(13), 5302–5308. <https://doi.org/10.1016/j.ijhydene.2013.02.012>
11. McDonald, J. E. et al. (2012). Methods for the isolation of cellulose-degrading microorganisms. In Gilbert, H. J. (Eds.). *Methods in Enzymology* (1st ed., Vol. 510). Elsevier Inc, 349–374. <https://doi.org/10.1016/B978-0-12-415931-0.00019-7>
12. Olabi, A. G. et al. (2021). Large-vs-scale hydrogen production and storage technologies: Current status and future directions. *Int. J. Hydrogen Energy*, 46(45), 23498–23528. <https://doi.org/10.1016/j.ijhydene.2020.10.110>
13. Duong, H. M. et al. (2020). Advanced thermal properties of carbon-based aerogels. In *Thermal Behaviour and Applications of Carbon-Based Nanomaterials*. Elsevier Inc, 221–269. <https://doi.org/10.1016/b978-0-12-817682-5.00009-x>
14. Singh, R. et al. (2020). Nanomaterials in the advancement of hydrogen energy storage. *Heliyon*, 6(7), e04487. <https://doi.org/10.1016/j.heliyon.2020.e04487>
15. Millet, P. (2014). Hydrogen storage in hydride-forming materials. In Basile, A. Adolfo, L. (Eds.). *Advances in Hydrogen Production, Storage and Distribution*. Woodhead Publishing Limited, 368–409. <https://doi.org/10.1533/9780857097736.3.368>
16. Zhao, Y. et al. (2021). Enhancing hydrogen storage properties of MgH<sub>2</sub> by core-shell CoNi@C. *J. Alloys Compd.*, 862, 158004. <https://doi.org/10.1016/J.JALLCOM.2020.158004>
17. Pyle, D. S. et al. (2016). Hydrogen storage in carbon nanostructures via spillover. *Int. J. Hydrogen Energy*, 41(42), 19098–19113. <https://doi.org/10.1016/j.ijhydene.2016.08.061>
18. Inkson, B. J. (2016). Scanning electron microscopy (SEM) and transmission electron microscopy (TEM) for materials characterisation. In Hübschen, G. Altpeter, I. Tschuncky, R. Herrmann H-G. (Eds.). *Materials Characterisation Using Nondestructive Evaluation (NDE) Methods*. Elsevier Ltd, 17–43. <https://doi.org/10.1016/B978-0-08-100040-3.00002-X>
19. Abhilash, V. et al. (2016). X-ray diffraction spectroscopy of polymer nanocomposites. In Thomas, S. Rouxel, D. Ponnamma, D. (Eds.). *Spectroscopy of Polymer Nanocomposites*. Elsevier Inc, 410–451. <https://doi.org/10.1016/B978-0-323-40183-8.00014-8>
20. Naderi, M. (2015). Surface area: Brunauer–Emmett–Teller (BET). In Tarleton, S. (Eds.). *Progress in Filtration and Separation*. Elsevier, 585–608. <https://doi.org/10.1016/B978-0-12-384746-1.00014-8>
21. Ishii, T. & Kyotani, T. (2016). Temperature programmed desorption. In Inagaki, M. (Eds.). *Materials Science and Engineering of Carbon*. Tsinghua University Press Limited, 287–305. <https://doi.org/10.1016/b978-0-12-805256-3.00014-3>
22. Huang, T. et al. (2021). Enhancing hydrogen storage properties of MgH<sub>2</sub> through addition of Ni/CoMoO<sub>4</sub> nanorods. *Materials Today Energy*, 19, 100613. <https://doi.org/10.1016/j.mtener.2020.100613>

23. Ji, Y. et al. (2020). Carbon aerogels with mutual support structures constructed by hybrid hydrogels: Robust energy storage materials. *Materials Today Communications*, 25, 101444. <https://doi.org/10.1016/j.mtcomm.2020.101444>
24. Dercz, G. et al. (2009). Structure studies on nanocrystalline powder of MgO xerogel prepared by the sol-gel method. *Mater. Sci. Poland*, 27(1), 201–207.
25. Montes, S. & Maleki, H. (2020). Aerogels and their applications. In Thomas, S. Sunny, A. T. Velayudhan, P. (Eds.). *Colloidal Metal Oxide Nanoparticles*. Elsevier Inc, 337–399. <https://doi.org/10.1016/b978-0-12-813357-6.00015-2>
26. Simón-Herrero, C. et al. (2016). Effects of freeze-drying conditions on aerogel properties. *J. Mater. Sci.*, 51(19), 8977–8985. <https://doi.org/10.1007/s10853-016-0148-5>
27. Mehrabi, M. et al. (2019). Surface structural alteration of multi-walled carbon nanotubes decorated by nickel nanoparticles based on laser ablation/chemical reduction methods to enhance hydrogen storage properties. *Int. J. of Hydrogen Energy*, 44(7), 3812–3823. <https://doi.org/10.1016/j.ijhydene.2018.12.122>